Characterization of the electrosprays of 1-ethyl-3-methylimidazolium bis(trifluoromethylsulfonyl) imide in vacuum

Manuel Gamero-Castaño
Department of Mechanical and Aerospace Engineering, University of California, Irvine, California 92717, USA

(Received 4 October 2007; accepted 19 February 2008; published online 31 March 2008)

The electrosprays of 1-ethyl-3-methylimidazolium bis(trifluoromethylsulfonyl) imide are composed of a complex mixture of ions and charged droplets, which can be analyzed to determine the structure of the beam and infer significant features of the electrohydrodynamic atomization. In particular, we use a combination of retarding potential and time of flight techniques to study these beams and are able to quantify the voltage drop along the cone jet, together with the velocity and diameter of the jet at the breakup location, confirm the strong influence of viscosity and electrification in the breakup, show that the electric field in and near the Taylor cone tip is insensitive to external electrostatic parameters, and study the spatial distribution of ions and droplets, whereby the paradoxical absence of ions in the outmost region of the beam is established. The research described in this article can be exploited in the modeling of capillary instability of charged jets: testing the results of these models is difficult, especially when nanojets are involved, and our findings and techniques provide the experimental support required by the theoretical activity. The present research is also applicable to the modeling of colloid thruster beams. © *2008 American Institute of Physics*. [DOI: 10.1063/1.2899658]

I. INTRODUCTION

The electrostatic atomization of liquids has been studied with recurring interest since the early work of Zeleny.[1] This phenomenon is relevant to processes requiring fine atomization, especially when a spray of charged droplets offers additional advantages such as the reduction of droplet coalescence or the means to control their trajectories. Some examples of these applications are spray combustion, dispensing of drugs, spray painting, and colloid thrusters.[2–4] In addition, this atomization technique coupled with common mass spectrometry detectors has enable the characterization of large macromolecules, resulting in the new field of electrospray mass spectrometry pioneered by Fenn *et al.*, the 2002 Nobel Prize laureate in chemistry.[5]

The technological potentiality of electrosprays has sparked interest in understanding the physics of the atomization process. Of the several electrospraying regimes identified in the literature the so-called cone-jet mode, characterized by its marked stability and atomization quality, is by far the better studied.[6,7] The problem is fluid mechanical in nature and its significant difficulty is compounded by the essential interaction with an electrostatic field, the transport of charge, the presence of a free surface, and a geometry with dimensions spanning many orders of magnitude. Typically a cone jet is induced at the tip of a conducting tube facing a second electrode, referred to as emitter and extractor. Liquid is fed to the emitter through its inner channel and a voltage difference between the electrodes established. If the flow rate and emitter potential are within certain limits, a stable cone jet will develop. Its main features, sequentially arranged downstream from the emitter, are a conical liquid meniscus (Taylor cone) attached to the emitter base, a transition region from which a jet emanates, a slender and accelerating jet with a length several orders of magnitude larger than its characteristic diameter, and a final region where the jet becomes unstable and breaks into charged droplets. When the physical properties of the liquid are such that nanometric jets and electric fields of the order of one Volt per nanometer are generated, ion field emission is triggered and the laws governing the cone jet become more complicated.[7,8]

The phenomenology of cone jets has been analyzed and modeled in different ways. Gañán-Calvo *et al.* derived for the first time (1993) asymptotic laws for the electrospray current and jet diameter using a model in which the charge relaxation time is much smaller than the hydrodynamic residence time (complete charge relaxation hypothesis).[9] Gañán-Calvo has refined this original analysis and successfully compared model and experimental results in subsequent work.[10–12] Conversely, Fernández de la Mora and Loscertales have explained the scaling law for the electrospray current by considering charge relaxation effects in the transition region between the Taylor cone and its jet.[13]

The breakup of a charged jet and the generation of droplets have been studied with both analytical linear models targeting the small deformation problem and numerical nonlinear models aimed at describing the full evolution into droplets. The numerous combinations of starting assumptions (e.g., whether viscosity is important or not, consideration of different electric field components, idealized electrification hypotheses, etc.) have generated a long list of limiting studies.[14] Recent large deformation analysis has used an equipotential electrification hypothesis, which is not valid for most cone-jet breakup cases.[15,16] The analysis of Gamero-Castaño and Hruby is specific to cone jets and may use a more adequate electrification hypothesis, but is re-

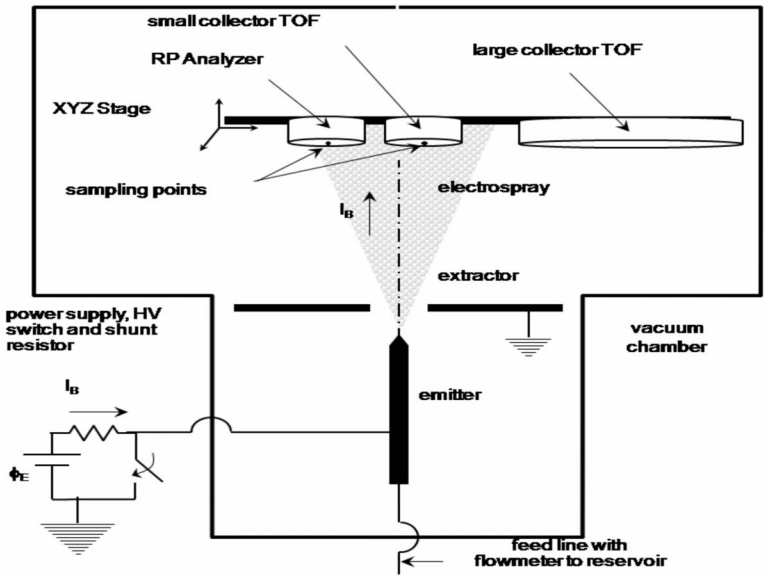

FIG. 1. Sketch of the experimental setup.

stricted to small deformations, it does not take into account charge relaxation effects, and its neglect of tangential electric fields is inconsistent.[17] The linear stability analysis of López-Herrera *et al.* use the more accurate leaky dielectric model to reproduce the effects of electrification[14] and considers a wide range of input jet parameters. In our opinion their framework and solutions are the most applicable to the real cone-jet breakup problem.[18] In general, the implementation of this body of theoretical work to electrospray applications is restricted by either the inaccurate modeling of electrification effects (especially in the more informative large deformation studies) or the imprecise knowledge of the state of the jet. Experimental information about the latter (e.g., the "undisturbed" jet radius and electrification level), and other key parameters such as droplet diameter and charge distributions, is most important to discern the relevant physics of the breakup and to demonstrate the results of theoretical models.

We present in this article retarding potential and time of flight techniques that expose with great detail the structure of the electrospray beams generated by the ionic liquid 1-ethyl-3-methylimidazolium bis(trifluoromethylsulfonyl) imide[19] (EMI-Im). The same techniques can be used to study the electrosprays of other liquids. This characterization is directly applicable to problems suh as the modeling of colloid thruster beams and the focusing of electrosprays for ion-beam-like applications. In addition, we analyze parameters of the beam particles to obtain important features of the cone jet: the voltage drop along the cone jet; the velocity, diameter, and potential of the jet at the breakup; and the insensitiveness of electrospraying variables to external electrostatic conditions. This information sheds light on the mechanics of the atomization process and should facilitate the accurate modeling of the breakup. The article is organized as follows: after this introduction an experimental section describes our setup, diagnostics, and raw data. Section III combines a simplified model of the cone jet and empirical data to analyze the latter, and to infer properties of the cone jet. Section IV summarizes our findings and outlines future research.

II. EXPERIMENTAL

Figure 1 shows a sketch of the experimental setup. The electrospray source has an axisymmetric triode configuration: the emitting anode is a platinum tube with a chamfered tip and inner and outer diameters of 0.16 and 0.48 mm, while the extracting cathode, made of a thin brass plate, has a 1.2 mm diameter orifice located 0.17 mm from the emitter; the beam of droplets exits the grounded extractor through its orifice and enters a larger area of the vacuum chamber where it is characterized. The opposite end of the platinum tube transitions into a fused silica capillary with the dominant hydraulic resistance to the flow, followed by a second fused silica tube used as a bubble flow meter. A reservoir storing EMI-Im outside the vacuum chamber feeds the flow meter. We control the pressure inside the reservoir to drive the desired flow rate. A high voltage power supply electrifies the emitter. A shunt resistor is used to monitor the beam current I_B. Unless otherwise specified, the potential of the emitter ϕ_E is 1700 V for all experiments described in this article. We study the sprays with a retarding potential analyzer (RPA) with a sampling orifice of 4.97 mm^2, a fast electrometer with an identical sampling area of 4.97 mm^2, and a second fast electrometer connected to a larger target. These electrometers measure the time of flight waves associated with either a small area of the beam or the whole beam, respectively. Time of flight waves are generated by suddenly shorting the emitter potential to ground with a high voltage switch, which interrupts the fluid atomization. The detectors are mounted on an *XYZ* positioning stage to sample the beam at different locations.

The density ρ, surface tension γ, viscosity μ, electrical conductivity K, and dielectric constant ε are the physical properties of EMI-Im relevant to this investigation. We have neither found nor measured the value of the dielectric constant. However, Ref. 20 reported values between 8.8 and 15.2 for five different ionic liquids with a comparable and/or equal cation, including the very similar 1-ethyl-3-

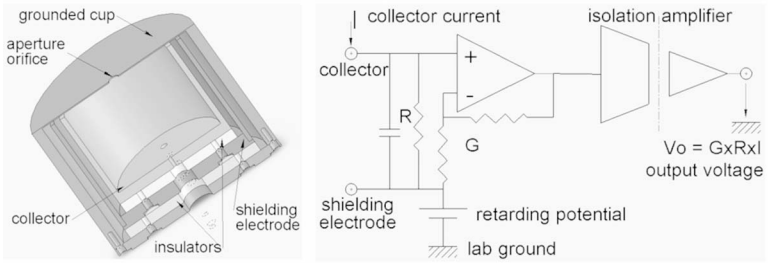

FIG. 2. Cross section of the retarding potential analyzer and diagram of its electric circuit.

methylimidazolium trifluoromethylsulfonate. Thus, a value of the order of 10 is probable for EMI-Im. For the other four properties we will use the values reported in Ref. 21: $\rho=1520\ \mathrm{kg/m^3}$, $\gamma=0.0349\ \mathrm{N/m}$, $\mu=0.034\ \mathrm{Pa/s}$, and $K=0.88\ \mathrm{S/m}$.

The retarding potential of a droplet ϕ_{RP}, defined as the sum of its kinetic and potential energies divided by the charge

$$\phi_{\mathrm{RP}} = \frac{1}{2\xi} v^2(\mathbf{x}) + \phi(\mathbf{x}), \tag{1}$$

remains constant in an electrostatic field. ξ stands for the charge to mass ratio of the droplet. Figure 2 shows our RPA and its electric circuit. The RPA is bounded by a cylindrical cup with an aperture orifice in the center of the base facing the electrospray. Charged particles enter through the aperture are exposed to the electric field induced by the grounded cup and the collector electrode, and an electrometer connected to the collector senses their charge. The retarding potential is applied at the collector electrode. Ideally, particles with a retarding potential infinitesimally larger than the potential of the collector will have, upon reaching the collector surface, a velocity vector parallel to the surface normal. In this case, the retarding potential of the analyzer and the retarding potential of the particle are equal, and a discontinuity in the measured current versus detector potential signals the event. This design aims at accurately measuring the retarding potential of beamlets with large entrance angles. We have confirmed this by solving numerically the electric field inside the analyzer and the resulting trajectories of charged particles, and comparing the retarding potential of the particle with the minimum detector potential preventing the deposition of the particle on the collector surface. In the analysis we use a beamlet of monoenergetic particles emitted from a point outside the detector and solve the particle trajectories as a function of the distance between the source point and the RPA aperture, the entrance angle formed by the beamlet axis and the aperture normal, and the point of entrance of the particle through the aperture. After computing trajectories with points of entrance throughout the orifice of the cup, we find that the mean of the ratio between the retarding potential of the beamlet and the collector potentials is close to 1 as long as both the entrance angle is smaller than 40° and the distance between the source and the RPA is larger than 3 cm (both conditions are met by most measurements in this article). Furthermore, under these conditions the standard deviation of the collector potentials is smaller than 2% of the beam retarding potential. This result is important because it provides an estimate of the resolution with which the retarding potential of polyenergetic beams can be determined.

Figure 3 shows a typical cumulative distribution generated by the RPA (current at the collector as a function of collector potential). We have divided the distribution in several zones to facilitate the description of its main features. The first peculiarity is the negative sign of the current at the beginning of zone 1, despite the positive polarity of the electrospray particles. This is caused by secondary electrons generated by the collision of beam particles with the grounded cup: beam ions cannot reach the collector because of their lower retarding potential and are turned back toward the grounded cup, with enough energy (approximately 1400 eV) to release secondary electrons. The secondary electrons then flow to the collector attracted by its positive potential. As the retarding potential of the collector is reduced, charged droplets begin to reach this electrode, and their positive charge offsets the current of secondary electrons. This dual contribution from charged droplets and secondary electrons shape zone 1. If the retarding potential is further decreased the curve displays a significant change in slope, which we use to define the beginning of zone 2. This new characteristic is indicative of a distinct group of particles, which happen to be ions. The distorting effect of secondary electrons is reduced once the ions reach the collector because the secondary electrons generated at the collector are likely to come back to this positive surface. At still lower retarding potential, i.e., in zone 3, the signal of the RPA slowly increases at a rate that

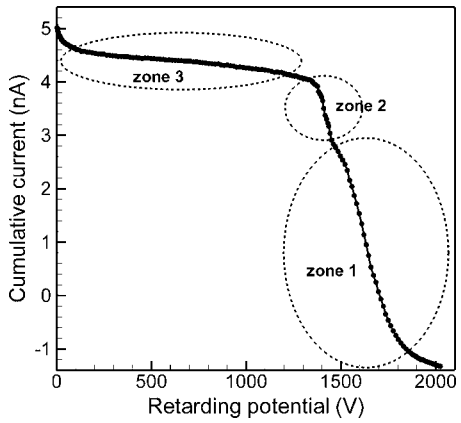

FIG. 3. Typical retarding potential curve. Charged droplets and ions are collected in zones 1 and 2, respectively. Zone 3 is the result of secondary electron emission from the RPA collector. The potential of the emitter is 1700 V.

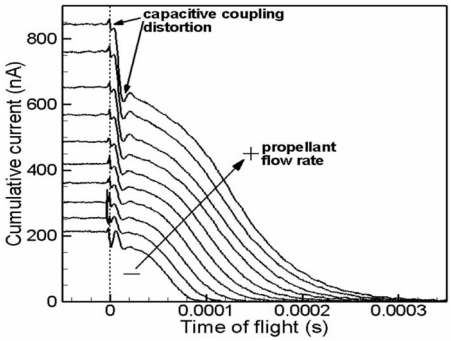

FIG. 4. Time of flight waves of entire electrospray beams. The sharp step near the origin is caused by singly charged ions, while the following and more gradual drop is due to charged droplets.

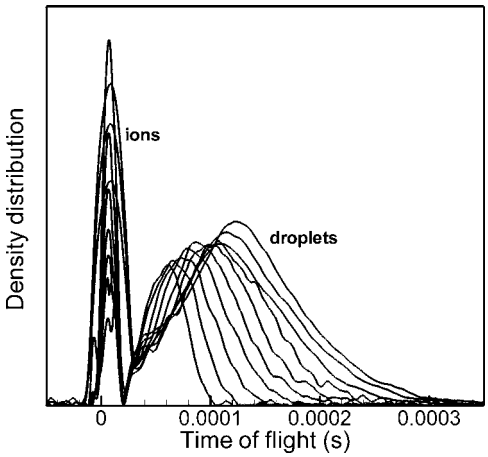

FIG. 5. Time of flight density distributions. The derivative of the cumulative distributions of Fig. 4, multiplied by −1, highlights the different ion and droplet populations.

becomes larger for decreasing retarding potential. We think that this feature is due to the distribution of energies of secondary electrons emitted from the collector, which have a higher probability of escaping the collector potential well as the depth of the well decreases. Additional data presented in the following paragraphs will support our identification of zones 1 and 2 with charged droplets and ions, respectively.

Figure 4 shows the time of flight waves of the overall electrosprays for several beam currents, recorded with the larger time of flight detector. This signal is the evolution of the current arriving at the collector after the sudden interruption of the atomization. The time origin, time of flight (TOF) =0 s, coincides with the interruption. The velocity of a particle is the ratio between the distance L_{TOF} separating the emitter and the collector and the TOF. The charge to mass ratio of the particle is determined from its velocity and retarding potential,

$$\xi = \frac{1}{2\phi_{\mathrm{RP}}}\left(\frac{L_{\mathrm{TOF}}}{\mathrm{TOF}}\right)^2. \tag{2}$$

All curves in Fig. 4 have two distortions near the origin unrelated to the actual TOF waves. They are caused by capacitive coupling between the emitter and the collector electrodes, i.e., it is an antenna effect of the electronics. Despite this problem, the structure of the TOF curves reveals two types of particles in every beam: fast ions with narrow velocity distributions and slower charged droplets with much wider velocity distributions. The narrowness of the former is due to the constrained charge to mass ratios that the ions can have, which is given by one unit charge, the mass of the EMI-Im cation, and maybe the mass of a predominant number of EMI-Im molecules (solvation state). The large velocity spread of the droplets is more evident in the density distribution representation of Fig. 5. Two features are worth pointing out: the distributions become broader for increasing beam current; and the charge to mass ratio of the droplets extends continuously up to values typical of individual ions. For the lower beam currents the latter observation could have been an artifact of the distortion of the signal. However, the TOF waves for the higher currents clearly do not have a void interval between ion and droplet regions, and therefore this appears to be a real trait of the electrosprays.

Figure 6 shows the profiles of three electrosprays with currents of 284, 540, and 746 nA. The profiles are measured in a plane perpendicular to the axis of the electrospray source, 12 cm downstream from the emitter tip. The profiles are not completely axisymmetric because of imperfections in both the emitter tip and the alignment of the emitter and the extracting electrode. This eliminates the usefulness of a more compact representation in spherical coordinates (i.e., using the polar angle instead of the radial position coordinate). The width of the beams increases with the electrospray current. We have sampled the radial positions identified by filled symbols with the RPA and the small TOF analyzer, and will describe the main findings next.

Figures 7 and 8 show retarding potential distributions and TOF waves associated with the 284 nA electrospray. The retarding potential curves for the three locations nearer the axis have two distinct particle populations, which will be identified as ions and droplets with the help of TOF analysis. The population with lower retarding potential (ions) is al-

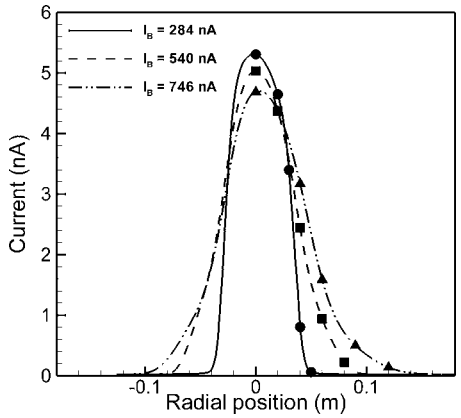

FIG. 6. Beam profiles for three different currents. These curves are constructed by sampling the beam current through a 4.97 mm^2 orifice, along a plane perpendicular to the axis of the electrospray source, 12 cm downstream from the emitter tip. The symbols identify locations studied in greater detail with the RPA and TOF analyzers, Figs. 7–12.

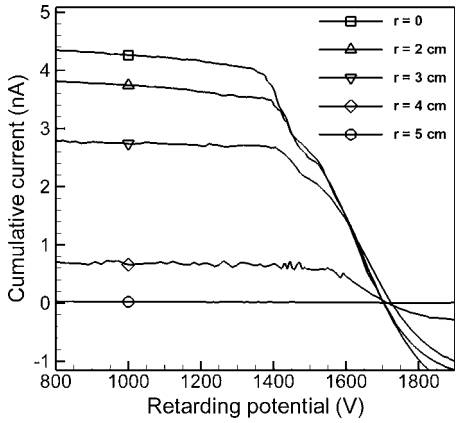

FIG. 7. Retarding potential cumulative distributions for the 284 nA beam measured at increasing separation from the beam axis. See Fig. 6 for the location of the samples in the beam profiles.

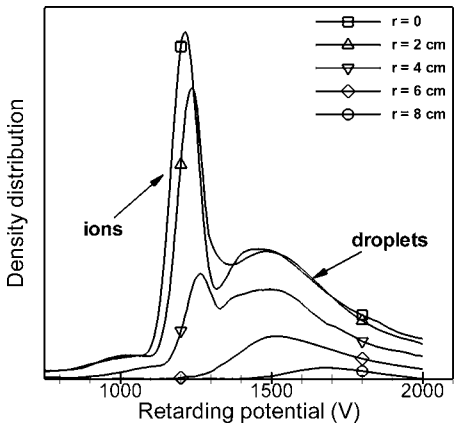

FIG. 9. Retarding potential density distributions for the 540 nA beam measured at increasing separation from the beam axis. See Fig. 6 for the location of the samples in the beam profiles.

most absent at a radius of 4 cm. The population with higher retarding potential (droplets) has similar retarding potential ranges anywhere in the beam. In Fig. 8, the axial coordinate is in units of TOF/L_{TOF} instead of TOF to account for the effect of increasing path of flight with increasing radius. Two features of these curves stand out: the current of ions in the TOF waves matches the height of the zone 2 of the retarding potential curves, which positively identifies the ionic composition of the latter; and the charge to mass ratio distributions of droplets are broad regardless of the radial position. The time resolution of our TOF electrometer is not good enough to determine the mass of the ions in these experiments. To achieve a current resolution of a fraction of 1 nA, we have used a capacitor as the input impedance of the electrometer ($I=CdV/dt$), rather than a resistor. A resistor is still needed to provide a path to ground for the bias current of the noninverting input of the operational amplifier, but its value has to be large enough (e.g., $R=1$ GΩ) so that the time constant RC (C is the capacitance of the collector, in our case of the order of the input parasitic capacitance of the operational amplifier) is much larger than the TOF of the beam particles. This imposes a stringent requirement in the maximum input bias current, and operational amplifiers satisfying this constraint have relatively poor dynamic responses. For example, we have used an Analog Devices' AD549K, which has an input bias current as low as 75 fA and a parasitic input capacitance of 1 pF, but exhibits a "poor" unity gain at 1 MHz and a 0.1% settling time of 4.5 μs. The last two characteristics are insufficient to accurately reproduce the TOF of the EMI-Im cations in our experiments, which is approximately 2 μs (75 amu, 1400 V acceleration voltage, 12 cm path of flight). It is worth noting that the accurate determination of the masses of the ionic species is not essential for this study, what is important is the capability to separate ionic and droplet populations.

Figures 9–12 show similar data for the 540 and 746 nA beams. The representation of the retarding potentials in terms of density distributions highlights three additional properties: the ions of a given beam have similar and narrow retarding potentials regardless of radial position (in particular, the maximum energies are nearly identical); the ions are absent from the outer region of the beam; and coinciding with the

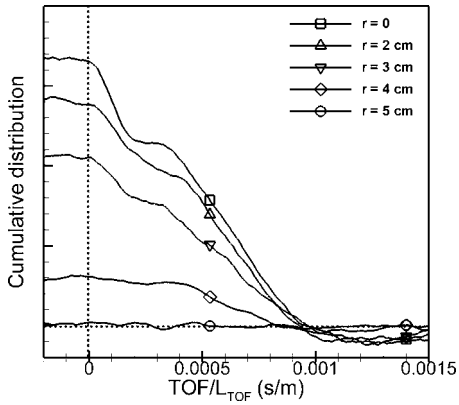

FIG. 8. Time of flight waves for the 284 nA beam measured at increasing separation from the beam axis. See Fig. 6 for the location of the samples in the beam profiles.

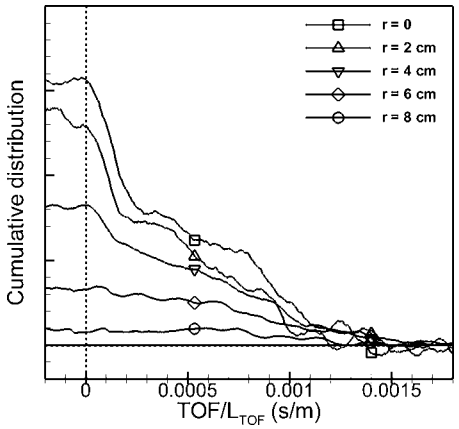

FIG. 10. Time of flight waves for the 540 nA beam measured at increasing separation from the beam axis. See Fig. 6 for the location of the samples in the beam profiles.

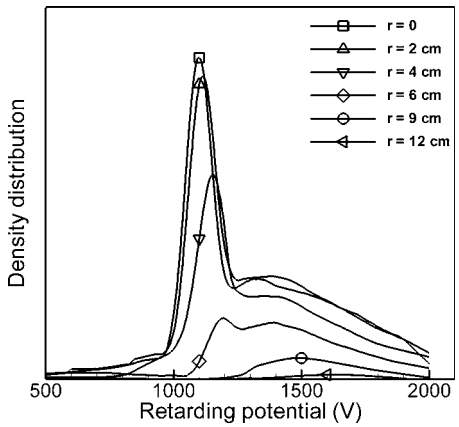

FIG. 11. Retarding potential density distributions for the 746 nA beam measured at increasing separation from the beam axis. See Fig. 6 for the location of the samples in the beam profiles.

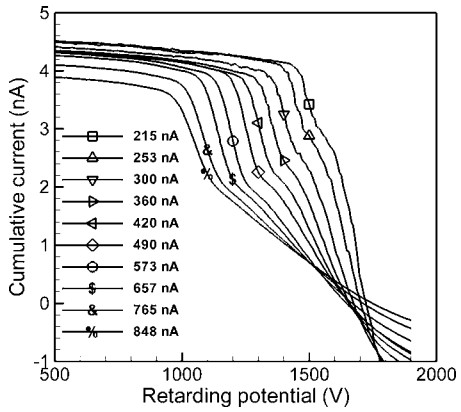

FIG. 13. Retarding potential distributions measured at the beam axis, for different beam currents and identical emitter potentials (1700 V).

disappearance of ions the droplet distributions slightly shift to higher retarding potential.

Figure 13 shows retarding potential distributions at the beam axis for different electrospray currents. The potential of the emitter is 1700 V in all cases. As the beam current increases the ions are less energetic, and the retarding potentials of droplets become broader.

Figure 14 plots retarding potential distributions measured at the axis of the beam for different emitter potentials and fixed flow rate. We have redefined the abscissa coordinate, $\phi_E - \phi_{\mathrm{RP}}$, in an attempt to factor out the changing value of the emitter potential ϕ_E. The new abscissa coordinate can be thought of a voltage deficit associated with the atomization process. The beam current is a weak function of the emitter voltage, as shown by the values included in the legend. The curves in Fig. 14 have the remarkable property of being largely independent of the emitter voltage: although the area under each curve does increase with ϕ_E (the profiles become narrower and more concentrated because of the increased axial velocities induced by larger acceleration voltages), the voltage deficits of the beam particles are virtually unchanged. In particular, it is striking that the minimum voltage deficit of the ions remains fixed at 450 V despite a 33% variation of the emitter voltage.

III. DISCUSSION

We begin this section with a qualitative description of the cone jet to provide the physical background for an explanation of the experimental phenomenology. Our understanding of cone jets is based on a model of three regions: the Taylor cone, a transition region between the cone and the jet, and the jet. The magnitudes of the electric and velocity fields in the cone are negligible because of the large cross sections available for the transport of mass and charge, and the laws of electrostatics and hydrostatics apply. In particular, the balance of stresses on the surface of the cone is simplified by solely retaining electrostatic and capillary stresses, and bulk conduction is the only important mechanism for the transport of charge. This static situation is violated wherever the fluid convection time, $t_f = r^3/Q$, becomes comparable to the electrical relaxation time, $t_e = \varepsilon\varepsilon_0/K$, a condition met near the cone vertex, $r \to 0$ (Q, K, and ε_0 are the flow rate, fluid electrical conductivity, and the vacuum permittivity). Thus, as the fluid approaches the tip of the cone the increased ve-

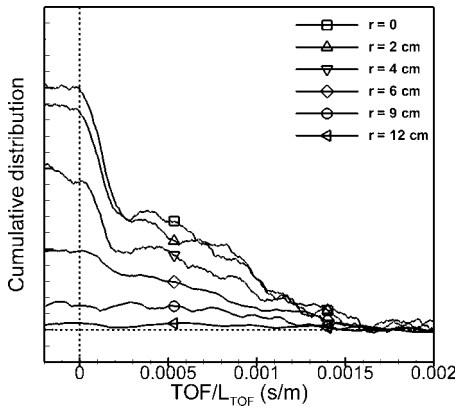

FIG. 12. Time of flight waves for the 746 nA beam measured at increasing separation from the beam axis. See Fig. 6 for the location of the samples in the beam profiles.

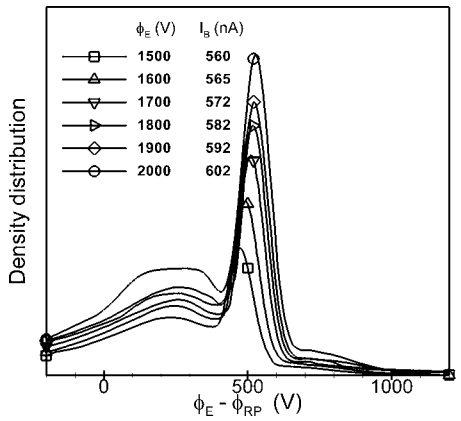

FIG. 14. Retarding potential distributions measured at the beam axis, for different emitter potentials and identical flow rates. The voltage deficit of ions, i.e., the emitter voltage minus the retarding potential, remains constant.

TABLE I. Relevant electrospray parameters directly measured or inferred from the experimental data: beam current I_B; fluid flow rate Q; jet charge to mass ratio ξ_J; voltage drop along the jet $\Delta\phi$; jet velocity at breakup v_J; jet diameter at breakup D_J; viscosity parameter J; Taylor number Ψ; characteristic viscous time t_μ; characteristic capillary time t_γ; length of the jet, z_J.

I_B (A)	Q (m^3/s)	ξ_J (C/kg)	$\Delta\phi$ (V)	v_J (m/s)	D_J (m)	J	Ψ	t_μ (s)	t_γ (s)	z_J (m)
2.15×10^{-7}	9.0×10^{-14}	1571	208	808	1.2×10^{-8}	2.7×10^{-4}	0.5	1.6×10^{-12}	9.6×10^{-11}	6.1×10^{-6}
2.53×10^{-7}	1.4×10^{-13}	1164	249	762	1.6×10^{-8}	3.5×10^{-4}	0.6	2.7×10^{-12}	1.4×10^{-10}	8.7×10^{-6}
3.00×10^{-7}	2.3×10^{-13}	875	296	720	2.0×10^{-8}	4.6×10^{-4}	0.7	4.5×10^{-12}	2.1×10^{-10}	1.2×10^{-5}
3.60×10^{-7}	3.6×10^{-13}	662	349	680	2.6×10^{-8}	5.9×10^{-4}	0.9	7.5×10^{-12}	3.1×10^{-10}	1.7×10^{-5}
4.20×10^{-7}	5.2×10^{-13}	531	397	649	3.2×10^{-8}	7.3×10^{-4}	1.1	1.1×10^{-11}	4.2×10^{-10}	2.2×10^{-5}
4.90×10^{-7}	7.5×10^{-13}	430	442	617	4.0×10^{-8}	9.0×10^{-4}	1.3	1.7×10^{-11}	5.7×10^{-10}	2.7×10^{-5}
5.73×10^{-7}	1.1×10^{-12}	351	508	597	4.9×10^{-8}	1.1×10^{-3}	1.6	2.5×10^{-11}	7.7×10^{-10}	3.6×10^{-5}
6.57×10^{-7}	1.5×10^{-12}	296	562	576	5.8×10^{-8}	1.3×10^{-3}	1.9	3.6×10^{-11}	1.0×10^{-9}	4.4×10^{-5}
7.65×10^{-7}	2.0×10^{-12}	246	625	554	7.0×10^{-8}	1.6×10^{-3}	2.3	5.3×10^{-11}	1.3×10^{-9}	5.6×10^{-5}
8.48×10^{-7}	2.6×10^{-12}	217	647	530	8.0×10^{-8}	1.8×10^{-3}	2.7	6.9×10^{-11}	1.6×10^{-9}	5.9×10^{-5}

locity field convects fluid with a surface charge lower than that required to fulfill the balance between capillary and electrostatic stresses, the tip charges below the level required to remain equipotential, and electric fields inside the fluid develop to inject charge on the surface and restore equipotentiality. In this area known as transition region the conduction current through the cone is gradually transformed into convected surface charge, a process which occurs relatively fast. This description, due to Fernández de la Mora and Loscertales,[13] emphasizes the importance of charge relaxation effects in the formation of the transition region. On the other hand, Gañán-Calvo offered an alternative model for the transition region by invoking the opposite limit of negligible charge relaxation effects. In this model the electrical relaxation time is always much smaller than the fluid convection time, and charge moves from the liquid bulk to the surface "instantaneously" to keep the surface charge in a state of quasiequilibrium.[22] Gañán-Calvo's analysis is applicable to cone jets operating at very large flow rates, which is likely the case of the present EMI-Im electrosprays. Regardless of the importance of charge relaxation in the transition region, we define the start of the jet as the point where surface charge convection becomes the only significant mechanism for charge transport. Hereafter the charge to mass ratio along the jet remains constant, and the fluid accelerates forced by the coupling between the electric field along the axis (largely induced by the distribution of charge on the Taylor cone) and the charge of the jet.[10] Eventually the jet becomes unstable and breaks into charged droplets. An approximate expression for conservation of momentum in the slender jet is

$$\frac{u(z)^2}{2}+\frac{p(z)}{\rho}+\xi_J\phi(z)=\text{constant}, \tag{3}$$

where u, p, and ϕ stand for the axial velocity, pressure, and potential along the jet. z is the axial coordinate. As mentioned before, the charge to mass ratio is constant, $\xi_J I_B/\rho Q$. The potential drop along the jet increases the kinetic energy and the pressure of the fluid. Equation (3) can be simplified by recognizing that, in the fluid traversing the jet, the variation of the pressure is much smaller than the drop in potential energy per unit volume. The pressure change is of the order of the capillary pressure near the jet breakup γ/R_J which can be compared to the voltage drop along the jet after scaling with the volumetric charge. We have used the jet parameters shown in Table I to estimate the resulting ratio $\gamma Q/(I_B R_J)$, which is between 2.9 and 3.2 V in our experiments. We will show that 3 V is a fraction of a percent of the typical voltage drop along the jet, and therefore the simpler balance between potential and kinetic energies is a good approximation,

$$\frac{u(z)^2}{2}\cong\xi_J[\phi_E-\phi(z)]. \tag{4}$$

In this expression the voltage drop along the transition region is neglected. For the highly conducting EMI-Im fluid this term should be small[23] and could be estimated with a better retarding potential characterization of the main droplets. Currently the distortion of zone 1 in the retarding potential curves caused by secondary electrons prevents us from doing so.

The ionic peak in the retarding potential curves provides several clues about the electrosprays. A cone jet has two regions from which ion field emission is more likely to happen: the transition region and the droplets at the jet breakup. At these two locations the normal component of the electric field reaches local maxima, and due to the exponential dependence of the emission rate on the repelling electric field, it follows that ions must be emitted from either one of these two regions.[8] To show this let us point out that in a jet where conduction current is negligible, the normal electric field increases with the jet radius,

$$E_{J,n}=\frac{I_B R_J}{2\varepsilon_0 Q}, \tag{5}$$

i.e., within the jet, the field increases in the direction toward the transition region (conversely, in the equipotential Taylor cone, Taylor's potential can be used to show that the normal electric field increases as one approaches the cone apex). On the other hand, using conservation of mass and charge inside the section of a jet evolving into a droplet, the ratio between the electric fields on the droplet and jet surfaces is proportional to the ratio between their radii,

$$\frac{E_{D,n}}{E_{J,n}} = \frac{2R_D}{3R_J}, \tag{6}$$

i.e., droplets with a radius 1.5 times larger than the terminal jet radius have an electric field larger than the jet. Ion field emission from the jet breakup has been demonstrated for electrosprays of formamide,[24] and it appears that most reported cases of ion emission from ionic liquids also belong to this modality. On the other hand, ion emission from the transition region, i.e., from the tip of the Taylor cone, has been observed for formamide and a few ionic liquids with large electrical conductivities and/or surface tensions.[8,21,25] The ions in these EMI-Im electrosprays are emitted from the jet breakup because, according to Fig. 13, they have potential deficits between 200 and 700 V, i.e., they are emitted at a potential well below that of the transition region (the only other possible ion-emitting area).

The velocity of an ion when it emerges from the liquid surface is the sum of its random thermal velocity and the velocity of the surface. Because the associated kinetic energy divided by the ion charge is a fraction of a volt, while the retarding potentials of ions in these sprays are over 100 V, it follows from Eq. (1) that the retarding potential of an ion is approximately equal to the potential of its point of emission, i.e., the breakup region in these electrosprays. The voltage deficit of the ions, $\phi_E - \phi_{\mathrm{RP}}$, combined with the narrowness of the ionic energy distributions and Eq. (4), makes it possible to define and estimate the velocity and diameter of the jet at the breakup,

$$v_J = \sqrt{\frac{2I_B}{\rho Q}(\phi_E - \phi_{RP})}, \tag{7}$$

$$D_J = \sqrt{\frac{4Q}{\pi v_J}}. \tag{8}$$

The ultimate velocity and diameter of the jet are key parameters in the study of cone jets and capillary breakup. These quantities are most difficult to measure, particularly in the case of submicrometric jets which are outside of the range of optical diagnostics. The fortunate emission of ions from the jet breakup, together with the measurement of their retarding potential and the current and flow rate of the electrospray, makes it possible to infer the elusive terminal velocity and diameter of our nanojets. Gamero-Castaño and Hruby have used a similar reduction technique to measure the diameter and velocity of submicrometric tributyl phosphate jets.[17]

Before proceeding any further let us compute several jet parameters with the measurements presented so far. Table I lists the fluid flow rate, the jet's charge to mass ratio, the voltage drop along the cone jet, the velocity of the jet, the jet diameter, the viscosity parameter and Taylor number, the viscous and capillary times, and the length of the jet, for different electrospray currents. The flow rate was measured directly with a bubble flow meter; the charge to mass ratio of the jet is the quotient of the beam current divided by the flow rate and fluid density; the voltage drop is the voltage difference between the emitter potential and the retarding potential of the ionic peak; the jet velocity is estimated with Eq. (7); and the jet diameter is computed with Eq. (8). The viscosity parameter J is defined as the square of the ratio between the viscous and capillary times ($\sqrt{J}$ is the inverse of the Ohnesorge number),

$$J = \frac{\gamma\rho R_j}{\mu^2} = \frac{\rho^2 R_j^4/\mu^2}{\rho R_j^3/\gamma} = \frac{t_\mu^2}{t_\gamma^2}, \tag{9}$$

while the Taylor number Ψ is the ratio between electric and capillary pressures,

$$\Psi = \frac{\sigma^2 R_j}{2\gamma\varepsilon_0} = \frac{I^2 R_j^3}{8Q^2\gamma\varepsilon_0}. \tag{10}$$

The jet diameters are a few tens of nanometers, reaching a value as low as 12 nm for the 215 nA beam. The voltage drop along the cone jet is a significant fraction of the emitter potential (1700 V), especially for the larger beam currents. Consequently, the fluid gains a considerable portion of its final velocity within the cone jet. It is worth noting that liquid velocities as high as 800 m/s are seldom attained by continuous liquid flows.

The most striking finding of this work is the lack of correlation between the voltage drop along the cone jet and the potential of the emitter at constant flow rate. Our interpretation of this result is that, as long as the emitter potential is within a range compatible with the formation of a stable cone jet, the axial electric field along the jet is unique and does not depend on the shape and potentials of the electrodes of the electrospray source. To prove this we use Eq. (4) to obtain the transit time t_J along the jet,

$$t_J = \int_0^{\phi_E - \phi_J} \frac{d\chi}{E_z\sqrt{2\xi\chi}}, \tag{11}$$

where E_z and χ are the axial electric field and a dummy variable representing the potential deficit along the jet, $\phi_E - \phi(z)$. A natural estimate for the transit time is the growth time of capillary disturbances. In this case, capillary instability theory indicates that t_J is determined by the fluid properties and flow rate. Thus, for fixed fluid conditions the definite integral in Eq. (11) must be a constant independent of the emitter potential, a property which according to Fig. 14 also applies to the upper limit of integration $\phi_E - \phi_J$. Although these two constraints do not eliminate a pathological relationship $E_z(\phi_E - \phi_J, \phi_E)$ consistent with a constant definite integral, the most realistic scenario is that of an axial electric field that does not depend on the emitter potential. Since the axial electric field along the jet is primarily induced by the distribution of charge near the Taylor cone tip, the observed independence on the emitter potential requires this distribution of charge to be mostly a function of the physical properties and flow rate of the fluid and largely decoupled from external electrostatic variables.

The local nature of the transition region of cone jets has been rationalized before. Like in the previous paragraph, this concept originated as an explanation for the remarkable independence of electrospray parameters such as the beam current and the droplet diameter on external electrostatic variables.[13,26] Our demonstration of the constancy of the po-

tential drop along the jet provides an experimental proof with a parameter that directly depends on the distribution of charge at the apex of the Taylor cone. Furthermore, it supports the use, pioneered by Gañán-Calvo,[10,12,27] of Taylor's potential to estimate the axial electric field accelerating the jet. For reference, we give Taylor's solution for the potential at the axis and the resulting estimates of the axial position and potential at the breakup as functions of the transit time,

$$\phi_T(z) = \phi_E - a_0(\gamma z/\varepsilon_0)^{1/2}, \quad a_0 = 1.3459, \tag{12}$$

$$z_J^{3/4} = (9a_0\xi/8)^{1/2}(\gamma/\varepsilon_0)^{1/4}t_J, \tag{13}$$

$$(\phi_E - \phi_J)^{3/2} = a_0^2(\gamma/\varepsilon_0)(9\xi/8)^{1/2}t_J. \tag{14}$$

Note that Eq. (12) yields the length of the jet as a function of the measured voltage drop along the jet. The last column of Table I collects these values, which range from 6 to 59 μm, i.e., from 500 to 780 jet diameters.

Our comments regarding Taylor's potential and the decoupling between voltage drop along the jet and electrostatic variables are the result of the large disparity of length scales in our electrospray source, i.e., the diameter of the jet and its length are much smaller than either the base of the Taylor cone or the separation between emitter and extractor electrodes.[27] In experimental conditions where the disparity of length scales is not fulfilled, the geometry and potentials of the electrospray source will have a substantial effect on the dynamics of the cone jet.

The linear theory of capillary instability accurately describes the initial stages of the jet breakup. The main result of this type of analysis is the so-called dispersion relation, or initial growth rate of sinusoidal perturbation modes as a function of the ratio between the perturbation wavelength λ and the undisturbed jet diameter D_J, and other dimensionless groups reflecting the relative importance of capillary, viscous, and electric stresses. The solution for the viscous and uncharged case is due to Chandrasekar,[28] who obtained the dispersion relation as a function of λ/D_J and the viscosity parameter J. Several extensions of Chandrasekar's problem to charged jets are marginally relevant to electrosprays because of the modeling of electrification phenomena. This is also true for all reported numerical simulations of the nonlinear, large deformation problem. The basic strategy adopted by these schemes is to use a simplifying electrification hypothesis like that of equipotential breakup, charge bounded to the jet surface, or constant volumetric charge, which may be appropriate for some limiting examples but fails to describe the general case. In our opinion the linear stability analysis of López-Herrera *et al.*,[18] which takes into account charge relaxation effects, is the most applicable to cone jets. However, we think that some features of this analysis such as the use of a surrounding cylindrical electrode, the neglected voltage drop along the cone jet, and its linear nature make difficult the extrapolation of its results to the breakup of cone jets. Although the existing theoretical solutions may not accurately quantify the effect of electrification on the capillary breakup of cone jets, the importance of the level of charging can be assessed by examining the Taylor number. Table I lists the Taylor numbers and viscosity parameters associated with these EMI-Im jets. The very large values of the Taylor numbers are striking. It is worth noting that the capillary pressure is fully balanced by the electrostatic pressure when the Taylor number is 1, $\Psi = 1$. A Taylor number larger than 1 is not compatible with the equilibrium of stresses on the jet surface, and we expect that charging at this level or higher will enhance and lead to instabilities. In fact, we think that a jet breakup with Taylor numbers this elevated cannot be axisymmetric (Gañán-Calvo brought to the attention of the author the likely nonasymmetric nature of the jet breakup): while solving numerically the axisymmetric breakup of charged jets, López-Herrera and Gañán-Calvo found that the results of their model for a jet with a Taylor number of 0.4 noticeably deviate from experimental results and attribute this divergence to the onset of a nonaxisymmetric jet breakup.[15] A nonaxisymmetric breakup is also consistent with the observed pattern of droplet generation in other cone jets. For example, Rosell and Fernández de la Mora report that (a) the droplet diameter distributions of lower conductivity fluids have the highest quality at the lowest flow rates (the sprays have a unique droplet population, commonly known as main droplet population); (b) a second, new droplet population (satellite droplets) appears together with the main droplets when the flow rate is increased beyond a critical value; and (c) after further increasing the flow rate the jet begins to oscillate, the diameter distributions become broader, and the sharp distinction between main and satellite populations disappear.[26] The same phenomenology has been described by Gamero-Castaño and Hruby using TOF and retarding potential techniques.[17] The latter authors measure a value of 0.3 for the Taylor number of jets generating main and satellite droplet populations, just before the onset of jet oscillations. Interestingly, 0.3 is close to the value of 0.4 reported by Ref. 15, and both of them are smaller than the Taylor numbers tabulated in Table I. Since the Taylor number increases with the flow rate for the cone jet of a given fluid [see Table I, Table 4 of Ref. 17, or use the scaling laws for the current and jet diameter, Ref. 10 and Eq. (10)], we expect that the onset of the jet oscillations observed by Rosell and Fernández de la Mora, and by Gamero-Castaño and Hruby, is associated with the surpassing of a critical Taylor number. Some implications of these observations to our EMI-Im electrosprays are clear: these jet breakups are not axisymmetric because of the elevated charge state of the jets; and the broad distribution of droplet velocities (see Fig. 4) and retarding potentials and therefore the likely broad distributions of droplets' diameters and charge values are the result of the inferior, nonaxisymmetric breakup.

The values of the viscosity parameters J in Table I are significantly smaller than those previously reported by Gamero-Castaño and Hruby for cone jets of moderately conducting solutions of tributyl phosphate.[17] In an axisymmetric breakup the wavelength of the disturbance that maximizes the dispersion relation increases for decreasing J, i.e., the ratio between the average droplet and jet radii, $\langle R_D \rangle / R_J$, increases as the breakup becomes more viscous. Although the breakup of these EMI-Im jets is not axisymmetric, this general trend is likely to continue and therefore we expect

$\langle R_D \rangle / R_J$ to be considerably larger than the value of 1.89 associated with the inviscid axisymmetric breakup.

It could be argued that the very large Taylor numbers would favor the formation of a pulsating, unstable jet. Such a scenario would jeopardy the analysis and results presented in this article, which require the existence of steady and orderly fluid acceleration and breakup. However, we think that the experimental evidence supports the existence of fully grown, permanent jet: the very narrow retarding potential distribution of the ions, and therefore the very narrow axial window from which ion emission takes place, seems incompatible with the stochastic nature of a pulsating jet.

Finally, the absence of ions in the outer region of these conical beams is a puzzling result. We have investigated previously the beams of less conducting fluids, which are typically formed by a mixture of main and satellite droplets and lack isolated ions. These beams display a spatial separation between the two families of droplets, with main droplets forming the inner core of the beam while satellites appear in a coaxial region surrounding the core. The separation is due to the smaller mass to charge ratio and initial inertia of the satellite droplets, which translate into a higher sensitivity to the space charge force pushing outward. The ions of the EMI-Im beams can be considered as a limiting case of satellite droplets in the sense that their mass to charge ratio and initial inertia are much smaller than those of any EMI-Im droplet, and by analogy the ions should predominantly appear in the outer section of the spray as well. We cannot offer at this point a reasoned explanation for the absence of ions at the largest spray angles. We think that the droplets emitting the ions are generated closer to the axis than nonemitting droplets, but we cannot explain how the nonaxisymmetric breakup causes this. We expect to resolve this paradox in future research.

IV. SUMMARY

We have used retarding potential and TOF techniques to characterize the electrosprays of the ionic liquid 1-ethyl-3-methylimidazolium bis(trifluoromethylsulfonyl) imide. These complex sprays are formed by populations of ions and droplets. Ions are emitted at the breakup region of the jet, from the surface of those droplets having the largest electric fields. The retarding potentials of the ions reveal the existence of a narrow axial window where the jet breaks into droplets and provides the electric potential for this region. The voltage drop along the cone jet, i.e., the emitter potential minus breakup potential, is significant and increases with the electrospray current (or equivalently with the flow rate). It varies from 208 to 647 V in the 215–848 nA current range. The voltage drop along the jet is insensitive to large variations of the emitter to extractor potential. This striking finding suggests that the charge distribution and electric field in and near the transition region of the cone jet do not depend on external electrostatic variables and support previous observations of a similar lack of dependence of the electrospray current and droplet diameter. Furthermore, the voltage drop along the cone jet, together with the fluid flow rate and beam current, yields the velocity and diameter of the jet at the breakup. The nanojet associated with the lowest electrospray current has a diameter and velocity of 12 nm and 800 m/s.

Surprisingly, the outer region of these electrosprays does not contain ions. This observation is paradoxical in view of the large charge to mass ratio and minimal emission inertia of ions compared to charged droplets.

We expect to use these findings and experimental methods to solve two problems of considerable importance: the quantification of electrification effects on capillary breakup and the modeling of colloid thruster beams. To the best of our knowledge, the large deformation instability problem including electrification laws consistent with cone jets has not been solved yet. Cone jets of different fluids provide the means of varying the important viscosity parameter by at least five orders of magnitude, while the Taylor number can be varied from irrelevant levels to values violating mechanical equilibrium. The numerical solution to this problem can be validated with measurements of the undisturbed jet diameter and the diameter and charge of droplets. We have presented here and elsewhere techniques for measuring the jet diameter. We have also developed an induction charge detector that measures both the diameter and charge of individual droplets, and which has a sensitivity of 100 electron charges.[29]

The second problem of interest to us is the modeling of colloid thruster beams. In particular, we are developing colloid thrusters using EMI-Im as propellant. A first principles model of the beam is important to optimize the design of the extracting electrodes and to determine the rate of propellant deposition on the thruster (key to assess thruster lifetime) and spacecraft surfaces (spacecraft contamination). The beam model requires two types of inputs to solve the equations of motion of particles: information about the distribution of particle parameters (charge to mass ratio is most important, while knowledge of diameters is desirable); and initial conditions in the form of particle initial velocities, position, and breakup potential. This information can be obtained with the experimental techniques presented here in combination with an induction charge detector.

ACKNOWLEDGMENTS

The measurements presented in this article were made during the author's previous employment at the Jet Propulsion Laboratory, Pasadena, CA, 91108.

[1] J. Zeleny, "The electrical discharge from liquid points, and a hydrostatic method of measuring the electrical intensity at their surfaces," Phys. Rev. **3**, 69 (1914).
[2] D. C. Kyritsis, S. Roychoudhury, C. S. McEnally, L. D. Pfefferle, and A. Gomez, "Mesoscale combustion: a first step towards liquid fueled batteries," Exp. Therm. Fluid Sci. **28**, 763 (2004).
[3] T. Ciach, "Microencapsulation of drugs by electro-hydro-dynamic atomization," Int. J. Pharm. **324**, 51 (2006).
[4] M. Gamero-Castaño, "Characterization of a six emitter colloid thruster using a torsional balance," J. Propul. Power **20**, 736 (2004).
[5] J. B. Fenn, M. Mann, C. K. Meng, S. K. Wong, and C. M. Whitehouse, "Electrospray ionization for mass spectrometry of large biomolecules," Science **246**, 64 (1989).
[6] M. Cloupeau and B. Prunet-Foch, "Electrostatic spraying of liquids. Main functioning modes," J. Electrost. **25**, 165 (1990).
[7] J. Fernández de la Mora, "The fluid dynamics of Taylor cones," Annu. Rev. Fluid Mech. **39**, 217 (2007).

[8]M. Gamero-Castaño and J. Fernández de la Mora, "Direct measurement of ion evaporation kinetics from electrified liquid surfaces," J. Chem. Phys. **113**, 815 (2000).
[9]A. M. Gañán-Calvo, A. Barrero, and C. Pantano-Rubiño, "The electrodynamics of electrified conical menisci," J. Aerosol Sci. **24**, S19 (1993).
[10]A. M. Gañán-Calvo, "Cone-jet analytical extension of Taylor's electrostatic solution and the asymptotic universal scaling laws in electrospraying," Phys. Rev. Lett. **79**, 217 (1997).
[11]A. M. Gañán-Calvo, "The surface charge in electrospraying: its nature and its universal scaling laws," J. Aerosol Sci. **30**, 863 (1999).
[12]A. M. Gañán-Calvo, "On the general scaling theory for electrospraying," J. Fluid Mech. **507**, 203 (2004).
[13]J. Fernández de la Mora and I. G. Loscertales, "The current transmitted through an electrified conical meniscus," J. Fluid Mech. **260**, 155 (1994).
[14]D. A. Saville, "Electrohydrodynamics: The Taylor–Melcher leaky dielectric model," Annu. Rev. Fluid Mech. **29**, 27 (1997).
[15]J. M. López-Herrera and A. M. Gañán-Calvo, "A note on charged capillary jet breakup of conducting liquids: experimental validation of a viscous one-dimensional model," J. Fluid Mech. **501**, 303 (2004).
[16]R. T. Collins, M. T. Harris, and O. A. Basaran, "Breakup of electrified jets," J. Fluid Mech. **588**, 75 (2007).
[17]M. Gamero-Castaño and V. Hruby, "Electric measurements of charged sprays emitted by cone-jets," J. Fluid Mech. **459**, 245 (2002).
[18]J. M. López-Herrera, P. Riesco-Chueca, and A. M. Gañán-Calvo, "Linear stability analysis of axisymmetric perturbations in imperfectly conducting liquid jets," Phys. Fluids **17**, 034106 (2005).
[19]A. B. McEwen, H. L. Ngo, K. LeCompte, and J. L. Goldman, "Electrochemical properties of imidazolium salt electrolytes for electrochemical capacitor applications," J. Electrochem. Soc. **146**, 1687 (1999).
[20]C. Wakai, A. Oleinikova, M. Ott, and H. Weingartner, "How polar are ionic liquids? Determination of the static dielectric constant of an imidazolium-based ionic liquid by microwave dielectric spectroscopy," J. Phys. Chem. B **109**, 17028 (2005).
[21]D. Garoz, C. Bueno, C. Larriba, S. Castro, I. Romero-Sanz, J. Fernandez de la Mora, Y. Yoshida, and G. Saito, "Taylor cones of ionic liquids from capillary tubes as sources of pure ions: The role of surface tension and electrical conductivity," J. Appl. Phys. **102**, 064913 (2007).
[22]A. M. Gañán-Calvo, "On the theory of electrohydrodynamically driven capillary jets," J. Fluid Mech. **335**, 165 (1997).
[23]M. Gamero-Castaño, "The transfer of ions and charged nanoparticles from solution to the gas phase in electrosprays," Ph.D. thesis, Yale University, 1999.
[24]M. Gamero-Castaño, "Electric-field-induced ion evaporation from dielectric liquid," Phys. Rev. Lett. **89**, 147602 (2002).
[25]I. Romero-Sanz, R. Bocanegra, J. Fernández de la Mora, and M. Gamero-Castaño, "Source of heavy molecular ions based on Taylor cones of ionic liquids operating in the pure ion evaporation regime," J. Appl. Phys. **94**, 3599 (2003).
[26]J. Rosell and J. Fernández de la Mora, "Generation of monodisperse droplets 0.3 to 4 μm in diameter from electrified cone-jets of highly conducting viscous liquids," J. Aerosol Sci. **25**, 1093 (1994).
[27]A. M. Gañán-Calvo and A. Barrero, "A global model for the electrospraying of liquids in steady cone-jet mode," J. Aerosol Sci. **27**, S179 (1996).
[28]S. Chandrasekhar, *Hydrodynamic and Hydromagnetic Stability* (Dover, New York, 1981), pp. 515–576.
[29]M. Gamero-Castaño, "An induction charge detector with multiple sensing stages," Rev. Sci. Instrum. **78**, 043301 (2007).